The Role of Current Collector in Enabling the High Performance of Li/S Battery

Almudena Benítez,[a] Prof. Álvaro Caballero,[a] Prof. Enrique Rodríguez-Castellón,[b] Prof. Julián Morales,[*,a] and Prof. Jusef Hassoun[*,c,d]

[a]Dpto. Química Inorgánica e Ingeniería Química, Instituto de Química Fina y Nanoquímica, Universidad de Córdoba, 14071 Córdoba, Spain.

[b]Dpto. de Química Inorgánica, Cristalografía y Mineralogía, Facultad de Ciencias, Universidad de Málaga, 29071 Málaga, Spain.

[c]Department of Chemical and Pharmaceutical Sciences, University of Ferrara, Via Fossato di Mortara, 17, 44121, Ferrara, Italy.

[d]National Interuniversity Consortium of Materials Science and Technology (INSTM) University of Ferrara Research Unit, University of Ferrara, Via Fossato di Mortara, 17, 44121, Ferrara, Italy

Summary

Among several factors, the nature of the current collector plays a significant role in determining the performance of Li/S battery. Carbon-based substrates gained recently increasing interest as alternative to conventional aluminum substrate. We show herein that cells based on sulfur-graphene composite reveal higher reversible capacity and lower polarization using carbon-based support rather than the typical aluminum current collector. The enhancement of cell performances is attributed to a decrease of electrode-electrolyte interphase resistance promoted by the use of carbon-support, as detected by electrochemical impedance spectroscopy (EIS) upon cyclic voltammetry (CV). This beneficial effect is ascribed to an improved contact of the active material particles with the support, and to increased electrode/electrolyte wetting due to its porosity and chemical nature, which are detected by Hg porosimetry, N_2 adsorption/desorption isotherms, SEM and X-ray photoelectron spectroscopy (XPS). Therefore, the results reported in this work

may be of interest for setting-up the most suitable condition for achieving high performance Li/S battery.

Introduction

1- Lithium Sulfur battery: the characteristics

Lithium battery is one the most promising energy storage systems for a wide variety of applications, ranging from modern portable electronics, to renewable plants and electric vehicles.[1-2] In this context, sulfur is gaining interest as electrode material due to its high theoretical specific capacity (1675 mAh/g) and energy density (2600 Wh/kg) provided by a multiple electron transfer between the light Li and S.[3,4] Furthermore, sulfur is abundant, and characterized by low-cost and environmental sustainability.[5-9] However, several issues, including capacity fading by cycling, low Coulombic efficiency and poor rate capability [10] hindered wide diffusion of the Li/S battery. These drawbacks, mainly due to poor conductivity of S, polysulfide shuttling, and loss of active material,[11] have been remarkably mitigated by moving to sulfur composite electrodes using a variety of carbons with different structures, textures and morphological characteristics,[12] and including polar species such as transition metal oxides.[13-15] Furthermore, electrolyte improvement [16-19] and, more recently, the use of an interlayer located between the cathode and the separator containing the electrolyte [20-22] have been proposed as suitable approaches for improving Li/S cell performances.

2- Lithium Sulfur battery: change of the electrode support

Very important factor influencing Li/S battery performance is the nature of the substrate used for the active material deposition, which actually improves the efficiency and the delivered capacity by the cell.[23-25] Indeed, we have reported in previous works a variety of optimized sulfur composites benefitting of carbon nanotubes,[23] and 3D-graphene with improved performances in terms of delivered capacity, rate capability and stability, which were well promoted by the employment of a carbon paper, i.e., a gas diffusion layer (GDL),

rather than conventional aluminum as the electrode support. In this work we attempt to shed light on the reasons for the beneficial effect of the support by using a N-doped 3D-graphene sulfur composite studied in our previous work [25] and prepared adopting procedures described in literature [26,27] in order to allow a full understanding of the optimal condition suitable for employing new and high performance sulfur electrodes in high-energy lithium battery.

Results and discussion

The evaluation of the electrochemical performance of the electrodes was made by combining of cyclic voltammetry (CV), galvanostatic cycling and electrochemical impedance spectroscopy (EIS). Fig. 1 (a, b) shows the CV curves of 3DNG-S using Al and GDL support, respectively. Both samples show during cathodic scan the two typical reduction peaks at about 2.3 and 2 V, corresponding to the conversion of S_8 ring to long-chain (Li_2S_x, $4 \leq x < 8$) and short chain (Li_2S_x, $x = 1,2$) lithium polysulfides, which are reversed during anodic scan into merged peaks at potential higher than 2.2 V, by multiple step oxidation process of the polysulfides into sulfur.[23-28] However, the cell using 3DNG-S cast into Al support (Fig. 1a) shows a different reaction kinetics, peak broadening, higher polarization, and lower current intensity with respect to the same sulfur composite cast onto GDL (Fig. 1b). This difference may be reasonably attributed to differences in conductivity and electrode wettability leading to higher charge transfer resistance between the two electrode configurations, as indeed well suggested by panels c and d of Fig. 1 reporting the EIS measurements recorded at OCV and after three voltammetric cycles. The two cells evidence a Nyquist plot containing a semicircles and a tilted line, which may be represented by a series of circuital elements including high-frequency ohmic electrolyte resistance (R_e), high-middle-frequency interphase resistances (R_i) and pseudo-capacitances (Q_i), and a low-frequency pseudo-capacitance (Q_g) accounting for semi-infinite Li^+ diffusion and capacitive behaviour of the cell.[29,30] The resistance values obtained by fitting the data

using the equivalent circuit reported in the insets of Fig. 1c and Fig. 1d, respectively, and Boukamp tool [31] are collected in Table 1. Beside the electrolyte resistance, which is typically constant for stable cells such as those reported by this work, significant differences between electrode/electrolyte interphase resistances are observed both at OCV and after three cycles. The electrode using Al support (Fig. 1c) shows an initial interphase resistance (R in Table 1) of about 40 Ω, which slightly increases to about 46 Ω upon cycles likely due to a solid electrolyte interphase (SEI) film consolidation.[30] Remarkably lower interphase resistance (R = 18 Ω) is observed for the 3DNG-S electrode using GDL support with respect to Al at the OCV (Fig. 1c). The resistance value becomes even lower after CV cycles of the 3DNG-S/GDL electrode (about 7 Ω), thus accounting for the low polarization observed in Fig. 1b, and for an activation process with a structural rearrangement of the electrode occurring by the ongoing of the electrochemical process.[29] Further proof accounting for electrode enhancement by using GDL support with respect to Al may be given by the SEM image in Fig. 1f and Fig. 1g, respectively, which reveal some missing contact between active material and Al support upon cycling (inset Fig. 1f), while remarkable morphological retention of the electrode using GDL (inset Fig. 1g).

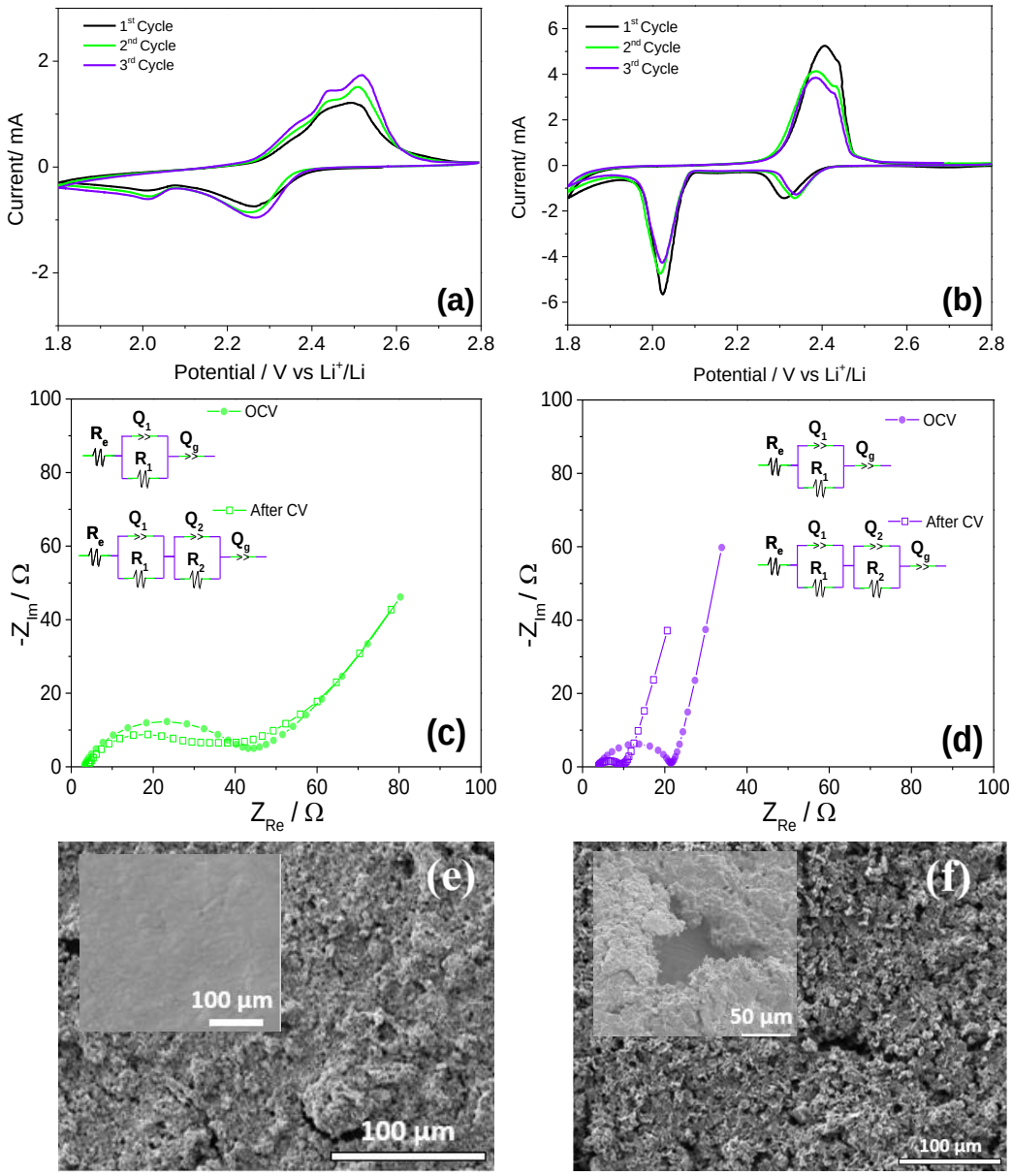

Figure 1. (a-b) Cyclic voltammetry profiles within the 1.8 – 2.8 V range with a scan rate of 0.1 mV s^{-1} of Li / DOL, DME (1:1), LiTFSI (1M), $LiNO_3$ (1M) / 3DNG-S cells using Al (**a**) and GDL (**b**) support for the 3DNG-S electrode. **(c-d)** Nyquist plots of the cells using Al (**c**) and GDL (**d**) support for the 3DNG-S electrode before and after recording the CV curves (third cycle). (**e-f**) SEM images of the 3DNG-S electrodes coated on **(e)** Al and **(f)** GDL current collectors before cycling and, in inset, after cycling. See experimental details in Supporting Information section for samples' acronym.

Cell condition	Circuit	R_1 (Ω)	R_2 (Ω)	$R = R_1 + R_2$ (Ω)	χ^2
3DNG-S/Al					
OCV	$R_e(R_{i,1}Q_{i,1})Q_g$	39.2 ± 0.7	-	39.2 ± 0.7	7.4×10^{-4}
After CV	$R_e(R_{i,1}Q_{i,1})(R_{i,2}Q_{i,2})Q_g$	28.5 ± 1.7	17.6 ± 1.2	46.1 ± 2.9	1.1×10^{-4}
3DNG-S/GDL					
OCV	$R_e(R_{i,1}Q_{i,1})Q_g$	18.2 ± 0.1	-	18.2 ± 0.1	1.8×10^{-4}
After CV	$R_e(R_{i,1}Q_{i,1})(R_{i,2}Q_{i,2})Q_g$	2.0 ± 0.5	5.3 ± 0.3	7.3 ± 0.8	3.2×10^{-4}

Table 1. Results of non-linear least square (NLLS) analyses [31] performed on the impedance spectra of Fig. 1(**c-d**) of the Li / DOL, DME (1:1), LiTFSI (1M), $LiNO_3$ (1M) / 3DNG-S cells using Al (**c**) and GDL (**d**) support for the 3DNG-S electrode at the OCV and after 3 voltammetry cycles. In detail: employed equivalent circuit, interphase resistance and χ^2 value of the fit. See experimental details in Supporting Information section for samples' acronym.

Figure 2 reports the steady state voltage profiles of Li/DOL, DME (1:1), LiTFSI (1m), $LiNO_3$ (1m)/3DNG-S cells using Al (a) and GDL (b) support. Both cells reveal the expected voltage signature, composed by two plateaus during discharge at about 2.3 and 2 V, and the corresponding plateaus during charge at about 2.2 V and 2.5 V, as already evidenced by cyclic voltammetry. The cell using the 3DNG-S on Al (Fig. 2a) shows satisfactory capacities of about 810, 770, and 700 mAh g^{-1} at C/8, C/5 and C/3 rate, respectively (1C = 1675 mA g_S^{-1}) with a polarization lower than 0.4 V. These good performances are relevantly improved by the employment of GDL as the cathode support (Fig. 2b), achieving the remarkable capacities of 1150, 1060, and 1000 mAh g^{-1} at C/8, C/5 and C/3 rate, respectively, and polarization lower than 0.2 V. It is worth mentioning that these performances are in line with our previous results on the 3DNG-S/GDL electrode using a different electrolyte media based on diglyme solvent.[25]

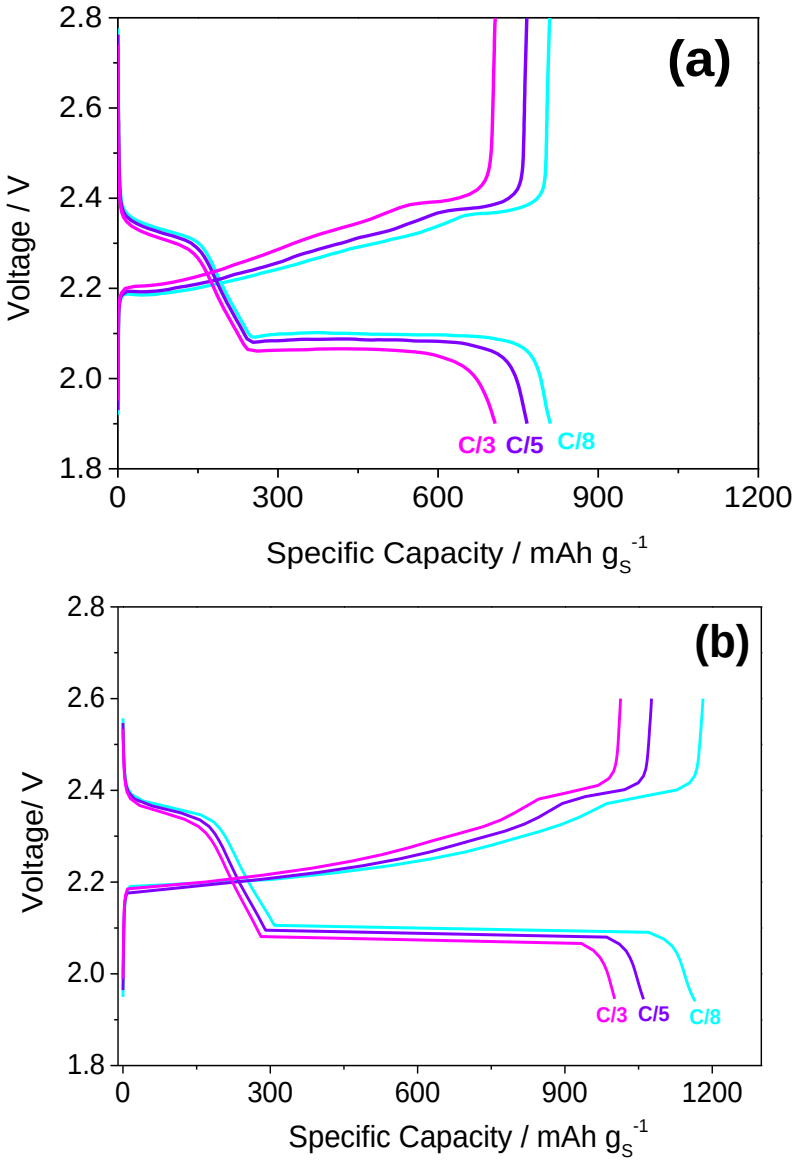

Figure 2 (a-b) Steady state galvanostatic cycling voltage profiles of a Li / DOL, DME (1:1), LiTFSI (1M), $LiNO_3$ (1M) / 3DNG-S cell using Al (**a**) and GDL (**b**) support for the 3DNG-S electrode at C/8, C/5 and C/3 rate (1C = 1675 mA g_S^{-1}). See experimental details in Supporting Information section for samples' acronym.

The improved electrode performances promoted by the GDL substrate may be attributed favorable surface morphology, porosity and the suitable chemical nature of the support as herein demonstrated by SEM, XPS and porosimetry. Figure 3 shows the SEM images of GDL (a) and Al (b) supports, and of the corresponding 3DNG-S electrodes (panels c and d, respectively). The GDL support shows remarkable roughness and the presence of free space represented by fractures of about 25 μm located between compact

carbon aggregates with a size of 250 μm, which represents a suitable characteristic for efficiently hosting the active material slurry (Fig. 3a); as expected, Al support reveals smooth surface and regular grooves mostly due to possible mechanical treatment (Fig. 3b). These differences are reflected into a more compact and uniform electrode using the GDL (Fig. 3c) with respect to that using Al which shows cracking and discontinuities (Fig. 3d). The improved electrode characteristics observed by SEM may actually enhance the contact between sulfur and carbon particles in the slurry, thus accounting for the lower resistance and better performances in lithium cell, as observed in Fig. 1 and Fig. 2.[32,33] Furthermore, detailed SEM images with increasing magnification (Fig. 3e, f) reveal the micrometric flakes of graphene containing sulfur, and super-P carbon which is one of the slurry components, that is, the electron conducting additive of the 3DNG-S electrode coated on GDL support.

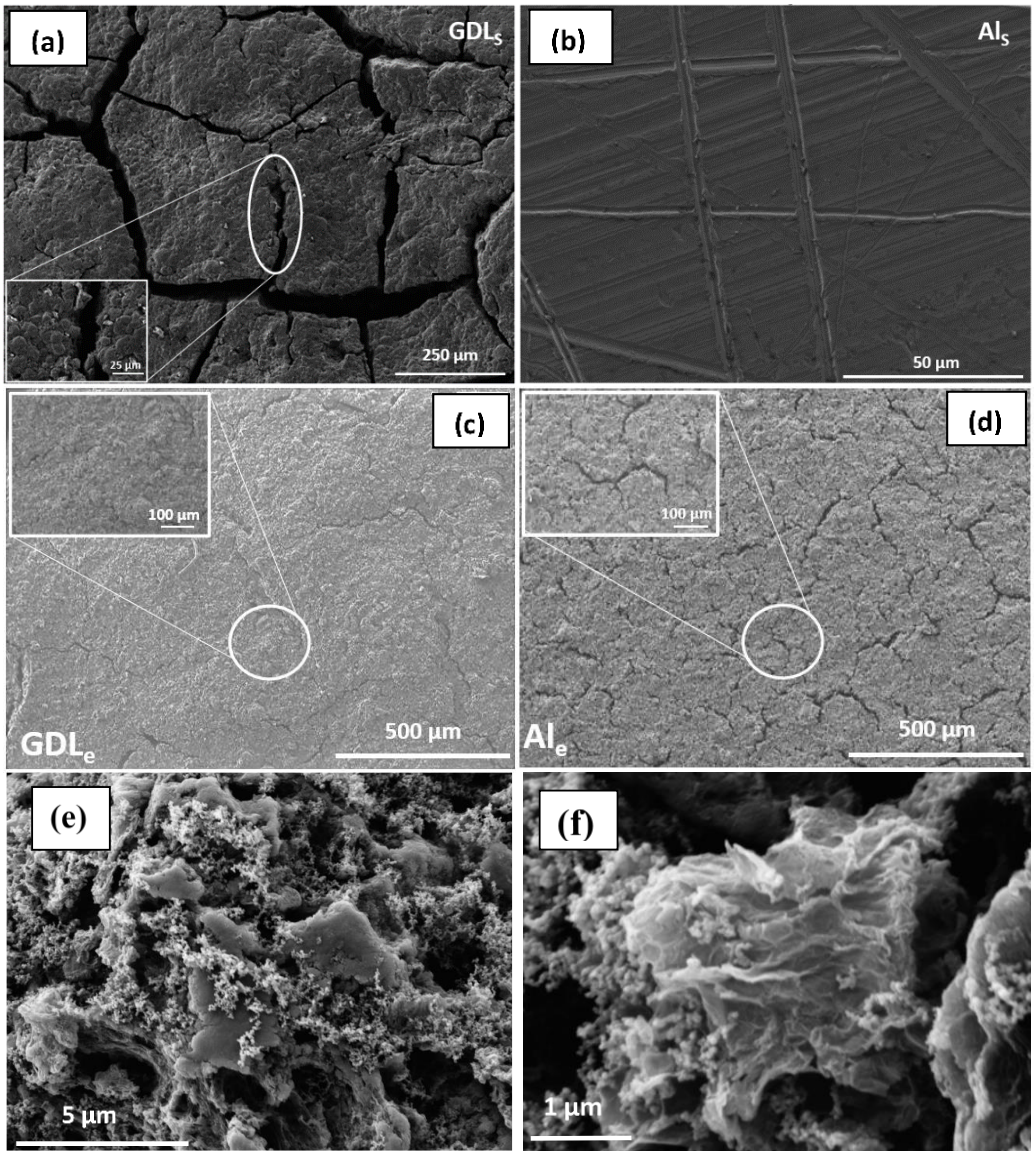

Figure 3. (a-d) SEM images at various magnifications of **(a)** GDL and **(b)** Al current collectors, and of the corresponding 3DNG-S electrodes (**c-d**, respectively). **(e-f**) SEM images with increasing magnification of the 3DNG-S material coated on the GDL support. See experimental details in Supporting Information section for samples' acronym.

Figure 4 shows the N_2-adsorption measurement of GDL support (a), Hg porosimetry (b, c) of AL and GDL supports, and XPS profile (d) of the GDL support. The N_2 adsorption/desorption isotherm (Fig. 4a) reveals a shape of type II and small hysteresis loop at a high relative pressure, above 0.9.[34] The data analysis indicates a BET surface area of 5 $m^2\ g^{-1}$, a pore volume of 0.04 $cm^3\ g^{-1}$, and a small micropore area of 0.3 $m^2\ g^{-1}$ which is consistent with an essentially macroporous nature of the GDL support, and a thin

layer coating of microporous carbon. The small hysteresis loop detected at high relative pressure (above 0.9) may be related to meso- macro-porous texture, which is further studied by Hg porosimetry. Macropore and mesopore volumes, V_{ma} and V_{me}, can be calculated bay taking into account the trend of pore cumulative volume (V_{cu}) versus pore radius (r) reported in Fig. 4 b, according to the approximations $V_{ma} = V_{cu}$ (at r = 250 A) and $V_{me} = V_{cu}$ (at r < 20 A).[35] The values of V_{ma} and V_{me} obtained for the GDL collector are of 0.298 and 0.0013 $cm^3\ g^{-1}$, respectively. The pore-size distribution (PSD) curve (i.e., dV/dlog(r) vs. pore radius) reported in Fig. 4c reveals pore dimensions ranging from 0.1 and 10 μm with a maximum at about 9 μm, which is in line with the SEM results (Fig. 3a). In contrast, Fig. 4(b, c) shows almost absence of porosity for Al as expected by the smooth surface of this support. In summary, we reasonably assume that the porous nature of GDL indicated by the above tests may enhance the 3DNG slurry characteristics with respect to the flat Al support, facilitate its impregnation by the electrolyte, and promote the Li/S reaction kinetics due to an improved charge- and electron-transfer at the electrode electrolyte interphase, as indeed observed in the electrochemical tests of Fig. 1. A further effect on the electrochemical reaction may be attributed to the chemical nature of the GDL which is revealed by XPS data of Fig. 4d. Besides the obvious presence of C (60.9%), the XPS detects also other elements such as F (38%), O (1%) and S (0.1%). The C1s photoemission signal reported in inset of Fig 4d is resolved in two main rather symmetric peaks with BE of 284.8 and 292.3. The first one corresponds to the carbon matrix of the substrate and the second to C bound to F (CF_2) [35] due to the Teflon-type component of the GDL. It cannot be excluded that the presence of these functional groups into the GDL can positively affect the kinetics of the electrochemical process, since electron attracting atoms such as F and O actually limit the polysulfide dissolution from the cathode to the electrolyte.[25] However further studies to clarify this aspect are required.

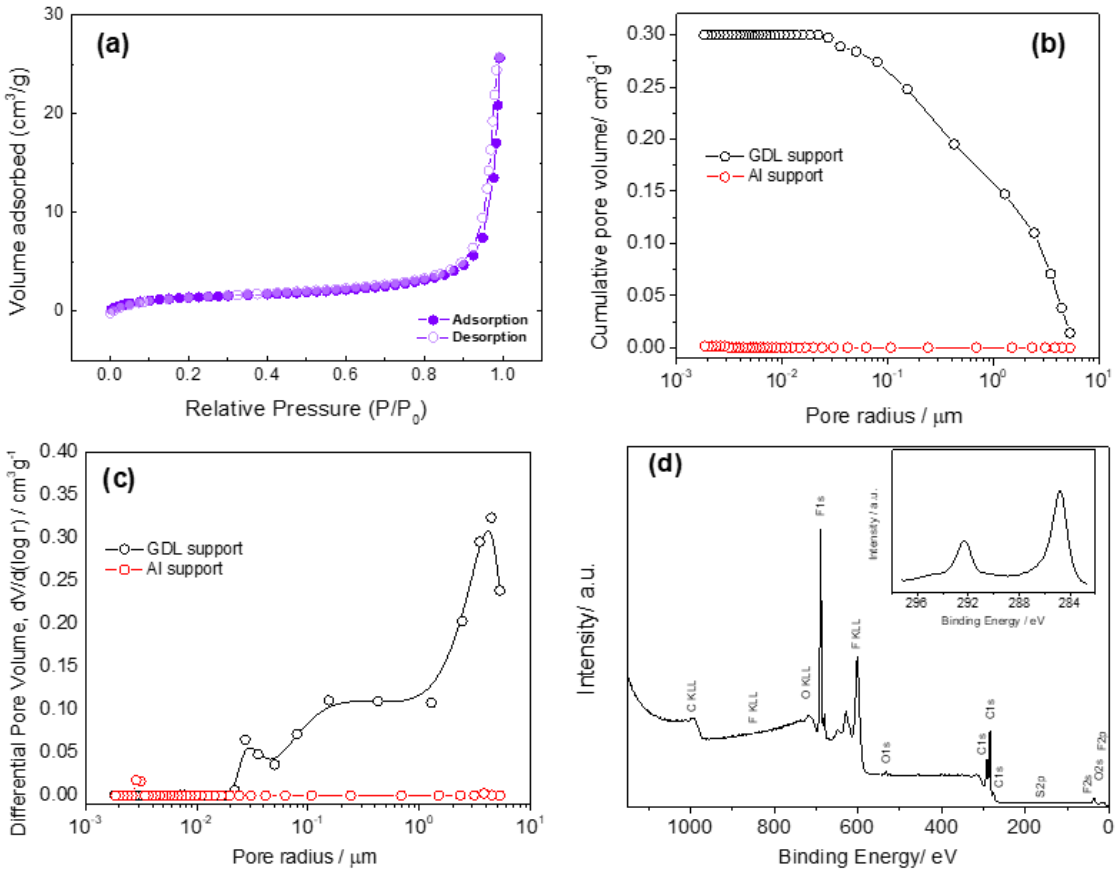

Figure 4. (a) N_2 adsorption/desorption isotherms for GDL substrate. (**b-c**) Variation of the cumulative pore volume with the pore radius **(b)**, and pore-size distribution (PSD) curve (dV/dlog(r)) **(c)** for Al and GDL current collectors**.** (**d**) XPS survey for GDL and C1s photoemission signal in inset.

The optimal combination of 3DNG-S and GDL is reflected into the improved cell performance of Figure 5 which shows the voltage profile (a) and the cycling response (b) of the Li / DOL, DME (1:1), LiTFSI (1M), $LiNO_3$ (1M) / 3DNG-S battery at a C-rate of C/5 (1C = 1675 mA g_S^{-1}). The figure reveals a very stable capacity for over 150 cycles (Fig. 5b), with a steady state value approaching 1000 mAh g_S^{-1}, delivered at an average working voltage of 2.1 V (Fig. 5a), thus leading to a theoretical energy density of about 2100 Wh kg_S^{-1}, and a practical value, calculated by taking into account inactive components such as current collector and cell case, exceeding 600 Wh kg^{-1}.[36] This excellent behavior is due to the synergic effect of an advanced sulfur composite benefitting of 3D graphene structure and nitrogen doping, i.e., 3DNG,[25] and a porous support which enables the best

performances of the latter, thus achieving the optimal condition for material operation in a high energy, and stable lithium-sulfur cell.

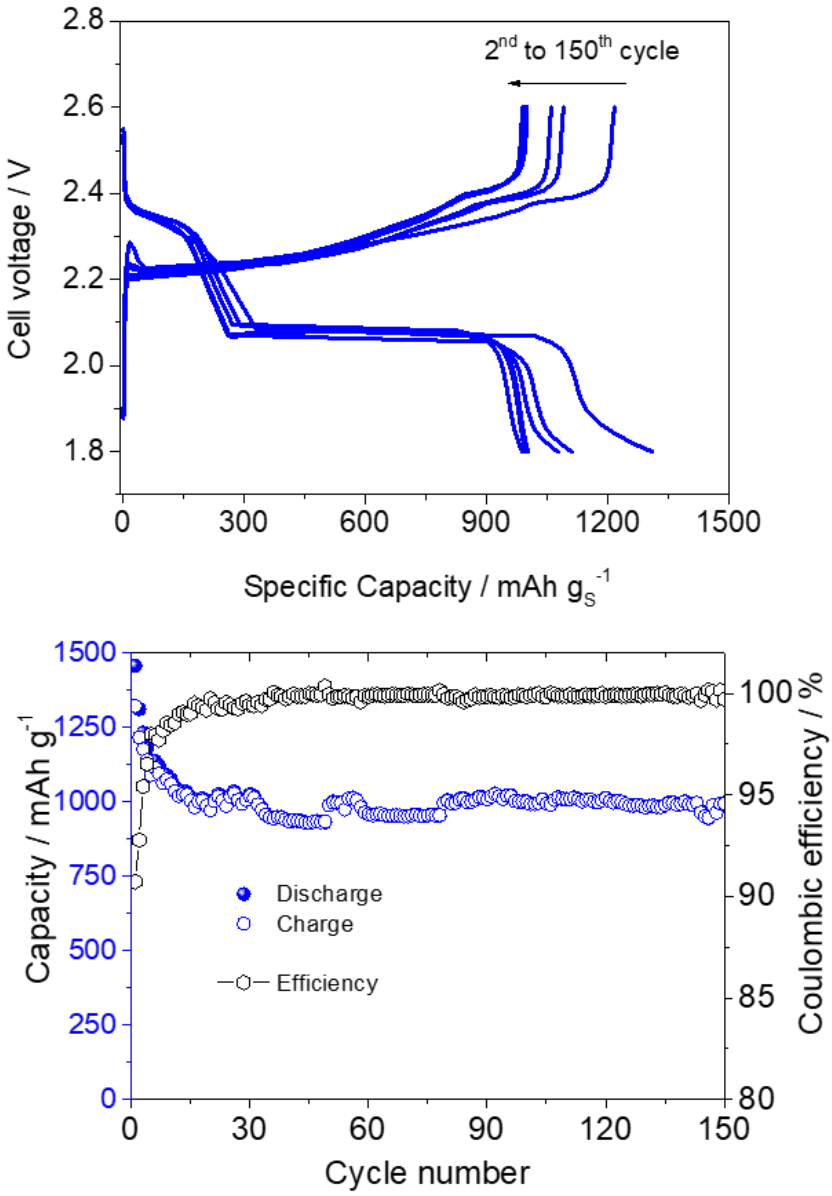

Figure 5 (a-b) Voltage profiles (**a**) and corresponding cycling trend with coulombic efficiency (**b**) of a Li / DOL, DME (1:1), LiTFSI (1m), $LiNO_3$ (1m) / 3DNG-S cell using GDL support for the 3DNG-S electrode at a current of C/5 (1C = 1675 mA g_S^{-1}). See experimental details in Supporting Information section for samples' acronym.

Conclusions

In this work we have investigated the effects of the electrode support on the performances of an advanced sulfur-graphene composite (3DNG-S) in Li/S cell. Electrochemical techniques (CV, EIS) evidenced a decreased cell polarization and interphase resistance, and suggested improved kinetics of the Li/S redox process by changing the support from conventional aluminum (Al) to a carbon-based gas diffusion layer (GDL). Carbon coated aluminum support has already been proposed for application in lithium battery due to improved conductivity and contact between support and active material.[37] However, this support differs only slightly with respect to aluminum in terms of porosity and ability for trapping polysulfide, since the carbon coating is generally constituted by a nanometric and very thin layer of carbon rather than micrometric porous substrate of the GDL used in this work.[38] For this reason, we focused our attention herein on the analysis of the enhancement of sulfur electrode performances observed by using the GDL support compared to conventional Al. Electron microscopy (SEM), N_2-adsorption and Hg-porosimetry indicated that the macroporous texture of the carbon-based substrate, rather than flat aluminum, leads to homogeneous distribution of the active particles, optimal contact with the current collector, high ionic and electronic conductivity, and favorable electrode wettability.[39] Furthermore, we have found possible positive influence on the electrochemical process of the chemical nature of the GDL, in which functional atoms such as F are detected by XPS. These characteristics have been reflected into very stable and performing Li/S cell, with reversible capacity of about 1000 mAh g_S^{-1} for over 150 cycles, and expected practical energy higher than 600 Wh kg^{-1}. The results suggested the use of the GDL as the preferred current collector in high performances lithium-sulfur battery.

Supporting Information Summary

The Supporting Information section reports the conditions adopted for the synthesis of the N-doped 3D-graphene/S electrode. Furthermore, this section indicates the conditions and the techniques used for the measurement, that is, scanning electron microscopy (SEM), N_2-

adsorbtion/desorbtion, X-ray photoelectron spectroscopy (XPS), mercury porosimetry, cyclic voltammetry (CV), electrochemical impedance spectroscopy (EIS) and galvanostatic cycling.

Acknowledgement

This work was performed with the financial support of the Ministerio de Economía y Competitividad (Project MAT2017-87541-R) and Junta de Andalucía (Group FQM-175). J.H thanks the grant Fondo di Ateneo per la Ricerca Locale (FAR) 2017, University of Ferrara.

Keywords

Battery; carbon-support; graphene; high-energy; lithium-sulfur

References

[1] A. S. Arico, P. Bruce, B. Scrosati, J. M. Tarascon, W. van Schalkwijk, *Nat. Mater.* **2005,** *4*, 366–377.

[2] J. B. Goodenough, Y. Kim, *Chem. Mater*. **2010,** *22*, 587–603.

[3] B. Scrosati, J. Hassoun, Y. K. Sun, *Energy Environ. Sci.* **2011**, *4*, 3287–3295

[4] A. Manthiram, Y. Fu, Y. S. Su, *Acc. Chem. Res.* **2012,** *46*, 1125–1134.

[5] Y. Yang, G. Zheng, Y. Cui, *Chem. Soc. Rev.* **2013,** *42*, 3018–3032.

[6] R. Xu, J. Lu, K. Amine, *Adv. Energy Mater*. **2015,** *5*, 1500408.

[7] R. Fang, S. Zhao, Z. Sun, D. W. Wang, H. M. Cheng, F. Li, *Adv. Mater.* **2017,** *29*, 1606823.

[8] H. J. Peng, J. Q. Huang, X. B. Cheng, Q. Zhang, *Adv. Energy Mater*. **2017,** *7*, 1700270.

[9] T. O. Ely, D. Kamzabek, D. Chakraborty, M. F. Doherty, *ACS Appl. Energy Mater*. **2018**, *1*, 1783–1814

[10] A. Manthiram, Y. Fu, S. H. Chung, C. Zu, Y. S. Su, *Chem Rev*. **2014**, *114*, 11751–11787.

[11] Z. Zeng, X. Liu, *Adv. Mater. Interface* **2018**, *5*, 1701274.

[12] Z. Li, Y. Huang, L. Yuan, Z. Hao, Y. Huang, *Carbon* **2015,** *92*, 41–63.

[13] S. Evers and L. F. Nazar, *Acc. Chem. Res.* **2013,** *46*, 1135–1143.

[14] Z. Li, J. Zhang, X. W. D. Lou, *Angew. Chemie Int. Ed.* **2015,** *54*, 12886–12890.

[15] N. Moreno, A. Caballero, J. Morales, E. Rodríguez-Castellón, *J. Power Sources* **2016,** *313*, 21–29.

[16] Z. Lin, Z. Liu, N. J. Dudney, C. Liang, *ACS Nano* **2013,** *7*, 2829–2833.

[17] M. Agostini, S. Xiong, A. Matic, J. Hassoun, *Chem. Mater*. **2015,** *29*, 4604–4611.

[18] M. Liu, D. Zhou, Y. B. He, Y. Fu, X. Qin, C. Miao, H. Du, B. Li, Q. H. Yang, Z. Lin, T.S. Zhao, F. Kang, *Nano Energy* **2016,** *22*, 278–289.

[19] K. Fua, Y. Gonga, J. Daib, A. Gonga, X. Hana, Y. Yaob, C. Wanga, Y. Wang, Y. Chen, C. Yanb, Y. Lib, E. D. Wachsmana, L. Hu, *PNAS* **2016,** *113*, 7094–7099.

[20] G. Zhou, S. Pei, L. Li, D. W. Wang, S. Wang, K. Huang, L. C. Yin, F. Li, H. M. Cheng, *Adv. Mater.* **2014,** *26*, 625–631.

[21] J. Q. Huang, T. Z. Zhuang, Q. Zhang, H. J. Peng, C. M. Chen, F. Wei, *ACS Nano* ***2015,*** *9*, 3002–3011.

[22] A. Wang, G. Xu, B. Ding, Z. Chang, Y. Wang, H. Dou, X. Zhang, *ChemElectroChem* **2016,** *3*, 1–8.

[23] L. Carbone, T. Coneglian, M. Gobet, S. Munoz, M. Devany, S. Greenbaum, J. Hassoun, *J. Power Sources* **2018,** *377*, 26–35.

[24] A. Benítez, D. Di Lecce, G. A. Elia, A. Caballero, J. Morales, J. Hassoun, *ChemSusChem.* **2018,** *11*, 1512–1520.

[25] A. Benítez, D. Di Lecce, A. Caballero, J. Morales, E. Rodríguez-Castellón, J. Hassoun, *J. Power Sources* **2018**, *397*, 102–112

[26] W. S. Hummers, R. E. Offeman, *J. Am. Chem. Soc.* **1958**, *80*, 1339–1339.

[27] H. Chen, C. Wang, W. Dong, W. Lu, Z. Du, L. Chen, *Nano Lett.* **2015**, *15*, 798–802.

[28] Y. S. Su, Y. Z. Fu, T. Cochell, A. Manthiram, *Nat. Commun*. **2013,** *4*, 2985−2991.

[29] L. Carbone, R. Verrelli, M. Gobet, J. Peng, M. Devany, B. Scrosati, S. Greenbaum, J. Hassoun, *New J. Chem.* **2016**, 40, 2935–2943.

[30] D. Aurbach, *J. Power Sources*, **2000**, 89, 206–218.

[31] B.A. Boukamp, *Solid State Ionics* **1986,** *20*, 31–44.

[32] W. Wahyudi, Z. Cao, P. Kumar, M. Li, Y. Wu, M. N. Hedhili, T. D. Anthopoulos, L. Cavallo, L. Li, J. Ming, *Adv. Funct. Mater.*, **2018**, 1802244.

[33] M. Li, Y. Wan, J. K. Huang, A. H. Assen, C. E. Hsiung, H. Jiang, Y. Han, M. Eddaoudi, Z. Lai, J. Ming, L. J. Li, *ACS Energy Lett.* **2017**, *2*, 2362–2367.

[34] K. S. W. Sing, *Pure & Appl. Chem.* **1982,** *54*, 2201-2218.

[35] M. Olivares-Marín, C. Fernández-González, A. Macías-García, V. Gómez-Serrano, *Energy & Fuels* **2007,** *21*, 2942-2949.

[36] J. Hassoun, K.-S. Lee, Y.-K. Sun, B. Scrosati, *J. Am. Chem. Soc.* **2011,** *133*, 3139–3143.

[37] I. Doberdò, N. Löffler, N. Laszczynski, D. Cericola, N. Penazzi, S. Bodoardo, G.-T. Kim, S. Passerini, *J. Power Sources*, **2014,** *248*, 1000–1006.

[38] S. Waluś, C. Barchasz, R. Bouchet, J.-F. Martin, J.-C. Leprêtre, F. Alloin, *Electrochim. Acta*, **2016,** *211*, 697–703.

[39] T.-G. Jeong, Y.-S. Lee, B. W. Cho, Y.-T. Kim, H.-G. Jung, K. Y. Chung, *J Alloys Compd* **2018**, *742*, 868–876

Table of content entry

Cells based on sulfur-graphene composite reveal higher reversible capacity and lower polarization using carbon-based support (GDL) rather than the typical aluminum current collector (Al). The benefits are herein ascribed to an improved contact of the active material particles with the support, and to increased electrode/electrolyte wetting due to its porosity and chemical nature, and detected by Hg porosimetry, N_2 adsorption/desorption isotherms, SEM and X-ray photoelectron spectroscopy (XPS).

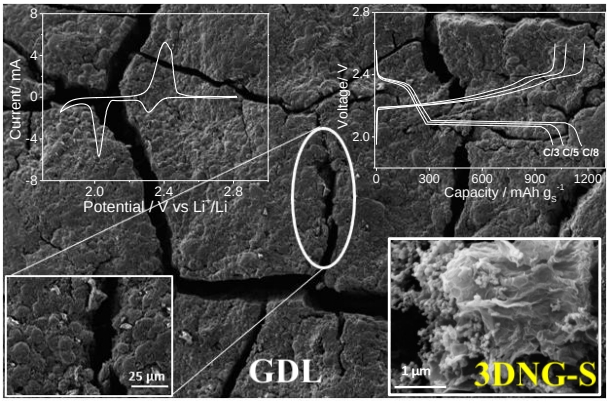

TOC graphic